ISSN 0016-7029, Geochemistry International, 2014, Vol. 52, No. 10, pp. 805–821. © Pleiades Publishing, Ltd., 2014.
Original Russian Text © A.I. Buikin, I.P. Solovova, A.B. Verchovsky, L.N. Kogarko, A.A. Averin, 2014, published in Geokhimiya, 2014, No. 10, pp. 867–884.

PVT Parameters of Fluid Inclusions and the C, O, N, and Ar Isotopic Composition in a Garnet Lherzolite Xenolith from the Oasis Jetty, East Antarctica

A. I. Buikin[a], I. P. Solovova[b], A. B. Verchovsky[c], L. N. Kogarko[a], and A. A. Averin[d]

[a] *Vernadsky Institute of Geochemistry and Analytical Chemistry, Russian Academy of Sciences, ul. Kosygina 19, Moscow, 119991 Russia*
e-mail: bouikine@mail.ru

[b] *Institute of the Geology of Ore Deposits, Petrography, Mineralogy, and Geochemistry (IGEM), Russian Academy of Sciences, Staromonetnyi per. 35, Moscow, 119017 Russia*

[c] *Open University, Walton Hall, Milton Keynes, MK7 6AA, United Kingdom*

[d] *Frumkin Institute of Electrochemistry, Russian Academy of Sciences, Leninskii pr. 31, bldg. 4, Moscow, 119071 Russia*

Received June 11, 2013; in final form, August 19, 2013

Abstract—Orthopyroxene, clinopyroxene, and olivine from a metasomatized mantle xenolith of garnet lherzolite in alkaline rocks at the Jetty Oasis, East Antarctica, contain numerous carbon dioxide-dominated composite melt–fluid and fluidized sulfide–silicate (±carbonate) inclusions. Although the maximum pressure under which the inclusions were captured by rock-forming minerals was evaluated at 13 kbar, its actual value should have been much higher, judging by the fact that the inclusions have lost part of their material (decrepitated) when the xenolith was brought to the surface. Two major fluid populations are distinguished. The fluids entrapped during the earlier episode have a more complicated composition. Dominated by CO_2, these fluids contain much N_2 (0.1–0.2 mole fractions), H_2S, and perhaps, also H_2O and are hosted by sulfide–silicate (±carbonate) inclusions produced by liquid immiscibility. As these inclusions evolved, they enriched in CO_2 and depleted in H_2S and N_2. Although the concentrations of N_2, H_2S, and H_2O were generally relatively low, these components played an important role in mantle metasomatism, as is reflected in the geochemistry of the derived magmas. The fluids of the younger episode (pressures lower than 7 kbar) are notably richer not only in CO_2 but also in H_2O (up to the appearance of inclusions with a liquid aqueous phase and the formation of CO_2 gas hydrate when cooled in a cryometric stage by liquid N_2). The effect of fluids on the mantle source in two discrete episodes is also confirmed by isotopic-geochemical data. Isotopic data on gases obtained immediately from fluid inclusions in minerals by the stepwise crushing technique provide evidence of the evolution of elemental and isotopic ratios of the gases in the course of the metasomatic processes. The high-pressure fluid inclusions of the earlier episode have low C/N_2, C/Ar, and N_2/Ar ratios, isotopically heavy N_2, and somewhat elevated (to 530) $^{40}Ar/^{36}Ar$ ratios. The younger fluids typically have higher (by two to three orders of magnitude) C/N_2 and C/Ar ratios, lower $\delta^{13}C$ of CO_2, and N_2/Ar and $^{40}Ar/^{36}Ar$ ratios close to the atmospheric values. The nitrogen and argon isotopic compositions and elemental ratios suggest that the younger fluids could have been produced by two-component mixing in the mantle–atmosphere system. Comprehensive analysis of the data and in particular the $^{40}Ar/^{36}Ar$ ratios, which are atypical of the mantle, and an increase in the H_2O concentration, suggests a subduction-related nature of the fluids.

Keywords: isotopes of light elements, noble gases, fluid inclusions, *P–T* parameters, mantle xenoliths, stepwise crushing

DOI: 10.1134/S0016702914100036

INTRODUCTION

The postaccretionary history of the Earth involved multiple episodes of mantle melting, which eventually produced the continental and oceanic crust. In the course of this process, the mantle should have continuously lost its low-melting and volatile components (CaO, Al_2O_3, TiO_2, trace lithophile elements, H_2O, and CO_2) and been transformed into a strongly depleted reservoir, from which only high-Mg melts depleted in trace elements could be derived afterward. However, this is at variance? with the tendencies detected in the Earth's geological evolution. Extensive factual materials obtained over slightly more than two past decades [1] demonstrate that mantle magmas become progressively enriched in incompatible elements. The analysis of our original databases reveals a remarkable increase in the intensity of alkaline magmatism with geological time [2].

This lately gave rise to ideas that the mantle and crust actively interact with each other [3], and this interaction is associated with large-scale material exchange and provides favorable circumstances for the development of mantle reservoirs enriched in trace lithophile elements and volatile components.

One of the most important geochemical consequences of the subduction of oceanic crustal material is mantle metasomatism, including carbonatisation. Thereby water and carbon dioxide are the major components of the fluid phase involved in mantle metasomatic reactions. The mantle beneath East Antarctica provides evidence of large-scale carbonate metasomatic processes. The zone of the Beaver rift system hosts a suite of ultramafic alkaline dikes and stocks (in the Prince Charles Mountains) that abound in xenoliths of mantle rocks: garnet lherzolites, dunites, and harzburgites. Their study has shown that the xenoliths contain carbonatized metasomatic domains cutting across the mantle material in the form of veinlets and consisting of clinopyroxene, olivine, spinel of a younger population, calcite, dolomite, high-Ba mica, apatite, and henrymeyerite [4]. One of the mantle xenoliths we examined consisted of garnet lherzolite with abundant fluid inclusions. The occurrence of fluid inclusions in the minerals testifies that a free fluid phase has been present at lower crustal levels and the upper mantle. Data on these fluids provides information on various evolutionary episodes of the volatile components with variations in the temperature and pressure and on the fluid regime of the system as a whole. Isotopic data obtained for gases released from fluid inclusions in rocks and minerals make it possible to identify the sources of the fluid and to trace the evolution of elemental and isotopic ratios of the gases in the metasomatic processes. Nowadays the most promising technique of gas extraction from fluid inclusions is stepwise crushing. This technique is proved to be efficient and successful in studying noble gases in mantle rocks [5–9 and others] and enables the researcher to conduct stepwise extraction of gases from fluid inclusions in rocks and minerals without involving gas components from the crystalline matrix of the minerals. This stepwise gas extraction, proceeding from the largest to smaller ones, and from the densest to less dens one (i.e., from weakly to more strongly "bound" in the structure), enables to obtain mixing lines in the isotopic diagrams to gain insight into the sources of the fluids of various populations. In view of the aforesaid, we have conducted a comprehensive isotopic-geochemical and microthermometric study of fluids in a unique sample of garnet lherzolite xenolith from the Oasis Jetty, Antarctica, with the aim of determining the sources of the fluids and clarifying their evolution during metasomatic transformations of the mantle beneath the East Antarctica.

METHODS

Inclusions in minerals from the xenolith were studied in a doubly polished thin section 0.3 mm thick. The experiments were carried out in a Linkam TS-1500 hot stage mounted at an Olympus (Japan) optical microscope, which was equipped with a digital photo camera, and in a small muffle furnace, which was used for long-lasting experiments at a specified temperature and subsequent rapid quenching of the inclusions after their heating. In the latter instance, in order to preclude oxidation of the Fe-bearing phases, we utilized graphite inserts. Fluid inclusions were examined in a Linkam-THMSG 600 heating/cooling stage, which can be cooled with liquid nitrogen (to −180°C) and was calibrated against standard reference synthetic inclusions with carbon dioxide and aqueous solutions of known concentration. The heating and cooling rates of the microthermometric experiments were controlled with the in-house software. The density of the fluids and the pressure were calculated with the FLINCOR computer program. Fluid inclusions were analyzed on a SENTERRA Raman spectrometer (Bruker) at the Frumkin Institute of Electrochemistry, Russian Academy of Sciences; the spectra were excited by a laser with a wavelength $\lambda = 532$ and 785 nm, power of 2- and 10 mW, respectively; the resolution of the spectrometer was ~3 cm^{-1}. The time of information accumulation was 100–1000 units depending on the types of the inclusions.

Solid phases were analyzed on a JXA-8100 (Jeol) electron microprobe at the Institute of the Geology of Ore Deposits, Petrography, Mineralogy, and Geochemistry (IGEM), Russian Academy of Sciences (analyst I. Griboedova) at an accelerating voltage of 20 kV, current of 20 and 30 nA, and electron beam 1, 2, and 5 μm in diameter. The standards were certified reference samples of natural minerals and glass: USNM 111240/2 (basaltic glass VG-2) for Si, Al, Fe, Mg, and Ca; jadeite for Na; orthoclase for K, rhodonite for Mn; TiO_2 for Ti; ZrO_2 for Zr; MgF_2 for F; vanadinite for Cl; $CuFeS_2$ for Cu, Fe, and S; Ni for Ni, Pt for Pt; Pd for Pd; Co for Co; and Ir for Ir.

The methods utilized to prepare samples for isotopic analysis of their gases were as follows. The samples were washed in ethanol in an ultrasonic bath to get rid of possible surface contamination and were then placed into a drying box for 2–3 hours. Upon their drying, the samples were loaded into a crushing tube connected with a vacuum line. The system was heated to 120°C and evacuated to high vacuum (10^{-8} torr) during one day to remove gases adsorbed on the surface. Gases for analysis were extracted from the samples by means of stepwise crushing. The gases obtained during each crushing step were cryogenically separated [10] and let into the chamber of the mass spectrometer for analysis of their isotopic compositions. Ar and He were additionally purified on Zr–Al getters. To get rid of possible interfering masses (first of all, CO), the nitrogen was additionally purified on CuO at 800°C. The CO_2 thus generated was

Table 1. Composition of dominant minerals of the xenolith

Component	*Ol*	*Opx*	*Cpx*	*Gr*	*Sp*	*Sp*
No.	1	2	3	4	5	6
SiO_2	40.82	54.13	52.05	41.92	0.12	0.09
TiO_2	0.00	0.14	0.41	0.11	0.26	0.09
Al_2O_3	0.06	5.58	6.71	22.66	52.95	62.75
Cr_2O_3	0.02	0.64	1.08	2.03	14.60	5.69
FeO	8.90	5.76	3.35	7.25	11.09	10.45
MnO	0.12	0.12	0.11	0.37	0.11	0.11
MgO	50.00	32.20	16.76	21.82	21.39	21.18
CaO	0.11	1.20	18.35	4.78	0.00	–
NiO	0.39	0.11	0.06	0.03	0.36	0.05
Na_2O	0.02	0.16	1.35	0.00	0.01	–
Total	100.44	100.04	100.22	100.97	100.89	100.40
mg#	0.91	0.91	0.90	0.84	0.77	0.78

trapped in a cold finger at a temperature of –170°C. The Ar and N isotopic composition in the gases extracted from an aliquot of monomineralic pyroxene separate was analyzed on a high-sensitivity Finesse mass spectrometric complex at the Open University in Milton Keynes, Great Britain, where data on the concentrations of He and C (in CO_2) were also obtained. It is important to emphasize that He, C, N, and Ar were analyzed simultaneously in a single portion of the gases extracted from the sample. The blanks were 0.6×10^{-8} cm^3/g, 4 ng, $0.5–3.7 \times 10^{-8}$ cm^3/g, and 1.25–7.6 ng for He, C, Ar, and N, respectively (the blanks for Ar and N depended on the extraction time). The technique is briefly described in [11].

The carbon and oxygen isotopic composition of carbon dioxide extracted from the whole-rock sample and olivine monomineralic separate was determined on a Thermo Finnigan Delta Plus mass spectrometer at the Vernadsky Institute of Geochemistry and Analytical Chemistry, Russian Academy of Sciences, using a microvolume cold finger, which provides reliable analysis of minor gas amounts (0.005–0.02 cm^3).

PETROGRAPHIC AND MINERALOGICAL OVERVIEW OF THE XENOLITH

The xenolith is $20 \times 15 \times 10$ cm. Garnet lherzolites found in the area are coarse-grained rocks with protogranular, locally porphyritic structures. The major rock-forming minerals are olivine, orthopyroxene, clinopyroxene, spinel, and garnet (Table 1). The olivine (forsterite, mg# = 0.903–0.906) contains 0.09–0.11 wt % CaO and up to 0.39 wt % NiO. The orthopyroxene and clinopyroxene have roughly the same mg#. The CaO concentration of the orthopyroxene is no higher than 1.20 wt %, and the Al_2O_3 concentration is 5.58–5.86 wt %. The garnet is dominated by the pyrope component (up to 77 mol %) and contains no more than 10 mol % grossular and almandine components each. The Cr_2O_3 concentration reaches 2 wt %, i.e., 5% of the uvarovite end member. The rock-forming spinel is high in Al_2O_3 (up to 53 wt %) and NiO and contains no more than 14.6 wt % Cr_2O_3 (Table 1, analysis 5).

The morphology of the phases testifies that the peridotite has been extensively reworked by metasomatic processes and has undergone a long-lasting evolution. Along with clear euhedral grains, the rock contains deformed (Fig. 1a) turbid an fractured orthopyroxene and olivine crystals. The marginal portions of clinopyroxene crystals are often resorbed (Fig. 1b) and bear worm-shaped glass (melt) inclusions containing up to 11 wt % CaO and 5 wt % Na_2O. Anhedral spinel grains are often resorbed and have a fine-grained texture. The orthopyroxene contains crystalline inclusions of orthopyroxene, garnet, and spherical inclusions of olivine (Fig. 1c). The compositions of olivine in the rock matrix and in inclusions are identical and have similar mg# = 0.904–0.906, respectively, and CaO concentration no higher than 0.1 wt %.

Along with the aforementioned phases, the xenolith contains large (up to a few millimeters) brown segregations (Fig. 1d). As can be seen under an optical microscope at a magnification of 1000–1500×, the segregations consist of mineral grains no larger than 30 μm across. Brownish platelets of high-Al spinel (up to 63 wt % Al_2O_3) with relatively low (compared to the phenocrysts) concentrations of Cr_2O_3 and NiO (6 and 0.05 wt %, respectively; Table 1, analysis 6) are submerged in a fine-grained mixture, in which we have analyzed orthopyroxene and Ca-enriched clinopyroxene. The inner texture of these segregations shows that their crystals grew perpendicular to the outlines of the segregations, and the segregations themselves are concentrically

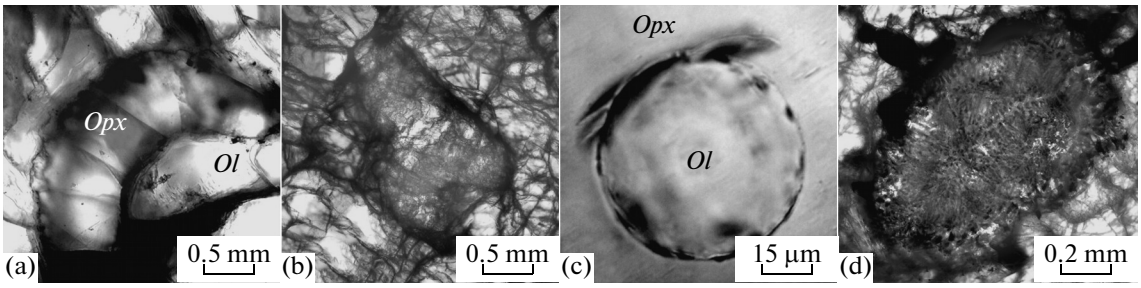

Fig. 1. Micrographs of the xenolith (transmitted light). (a) Deformed orthopyroxene crystal. (b) Resorbed clinopyroxene crystal with a dark secondary alteration rim. (c) Spherical olivine inclusion in orthopyroxene. (d) Altered garnet surrounded by a kelyphite rim. Scale bars are shown in each micrograph.

zoned. They resemble kelyphitic rims replacing grains of garnet outside its thermodynamic stability field and/or during its interaction with fluid or melt [12]. The hypothesis that our segregations are produced by an analogous mechanism receives further support from the fact that the orthopyroxene contains single-crystal inclusions (up to 120 μm across) whose optical characteristics correspond to garnet.

RESULTS AND DISCUSSION

Study of Inclusions

Types of microinclusions in minerals. The dominant minerals of the xenolith (orthopyroxene, olivine, and clinopyroxene) contain abundant inclusions of various types: (I) melt inclusions, (II) fluid inclusions, (III) composite inclusions, (IV) fluid–sulfide–silicate–carbonate inclusions, and (V) fluid inclusions coexisting with the fluid–sulfide–silicate–carbonate inclusions. All inclusions are very small (2–5 μm), but the minerals occasionally contain larger (up to 10 μm) vacuoles. The halos of partial material loss from the inclusions classed with types (II) through (V) were produced by the partial leaking of the inclusions (their decrepitation) in response to decompression when the xenolith were entrained to the Earth's surface by magmas. As a result of decrepitation, inclusions of different density may simultaneously occur in the same zones.

Melt inclusions of type I (Fig. 2a) were detected in the clinopyroxene. They contain glass and a gas bubble (which makes up no more than 7% of the inclusions by volume). Most of the inclusions occur in the marginal zones of resorbed crystals, although single melt inclusions were also found in clear intermediate portions of zoned clinopyroxene crystals.

Fluid inclusions of type II are either primary or secondary. Most of the inclusions are two-phase and consist of gas and liquid (Fig. 2b). At room temperature, the primary inclusions often contain only liquid. Both the primary and secondary decrepitated inclusions occurring along cracks sometimes contain up to 80 vol % gas (occasionally even more) and rarely also contain carbonate crystals (Fig. 3a). Carbonate phases were also identified in the composite (with fluid) secondary inclusions (Figs. 3b, 3c) and as newly formed crystals in the interstitial space between rock-forming minerals (Fig. 3e). In some inclusions of type II, we have found and examined solid segregations consisting of two liquids (H_2O and CO_2) and gas (Fig. 2e).

Composite melt–fluid inclusions (type III) bear partly or completely recrystallized melt and two-phase fluid (liquid and gas) (Figs. 2c, 2d, and 2f). Minute cracks cutting across these inclusions usually do not extend outside the host mineral grains, a fact suggesting that these cracks were produced *after* the inclusions had been entrapped. These inclusions were classed with the primary ones.

It is worth mentioning droplet- and 8-shaped sulfide–silicate (±carbonate phase) fluid-bearing inclusions of type IV (Fig. 4), which occur as clusters in orthopyroxene and olivine crystals. It can be seen under a microscope that the surface of the sulfides is pitted with caverns, which were formed when fluid segregations were opened and their material leaked when the polished thin sections were prepared. These inclusions are surrounded by leakage halos with tiny fluid inclusions of analogous composition. Considered together with the rounded shapes of the inclusions, the scatter of their material within halos in the host minerals suggests that minute portions of the material of these inclusions were entrapped in a liquid state.

Analysis of the sulfides indicates that droplets of monosulfides solid solution with a variable metal/sulfur ratio (0.77–1.04) and notable variations in the concentrations of the metals (15–31 at % Fe, 14–28 at % Ni, negative-7 at % Cu, and 0.2–0.6 at % Co) may sometimes simultaneously occur within a single cluster of the inclusions. In one instance, we have analyzed two sulfide phases with (Ni + Co)/(all metals) ratios of 0.33 and 0.57. According to experimental data [15], such sulfide globules can be interpreted as sulfide melt with a liquidus temperature between 1000 and 1050°C. At the same time, according to [14, 15], these correspond to the compositions of Ni-enriched monosulfides solid solution at 950–1000°C. The silicate component of the inclusions consists of fine-grained aggregates (Fig. 4b),

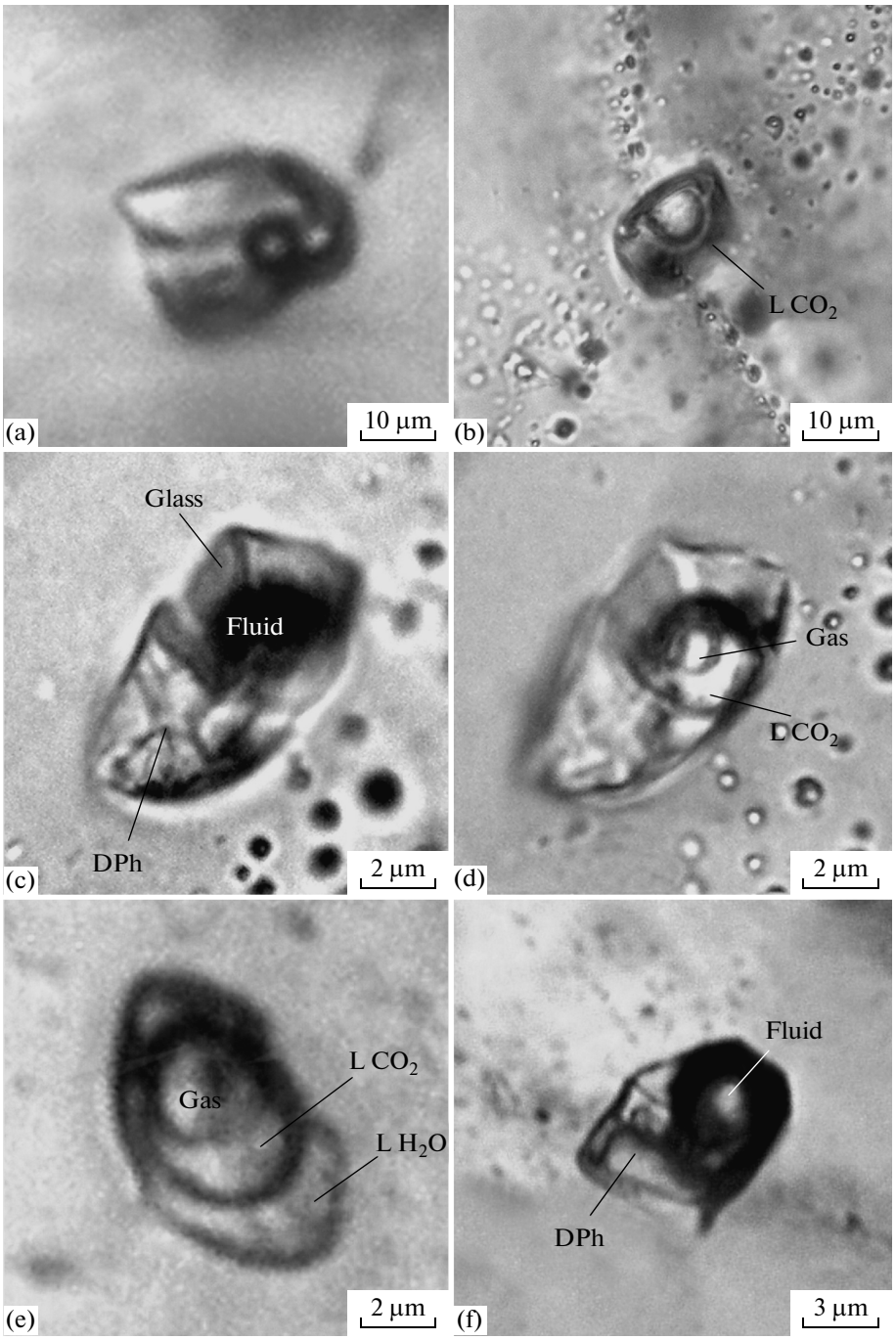

Fig. 2. Micrographs of inclusions in various minerals of the xenolith (transmitted light). (a) Melt inclusion in clinopyroxene, contains glass, crystalline phases, and a fluid phase. (b) Partly decrepitated large fluid inclusion at an intersection of cracks that do not extend outside the host mineral grain. (c, d) Composite melt–fluid inclusion in orthopyroxene (the micrograph shows the same inclusions at focusing at various depths). The inclusion contains (c) crystalline phases, glass, and (d) two-phase fluid. (e) Three-phase fluid inclusion with two liquid phases (H_2O and CO_2) and a gas bubble. (f) Composite melt–fluid inclusion with a large daughter crystal, glass, and fluid.

Symbols: L—liquid, Glass–silicate glass, Fluid—liquid + gas, DPh—daughter phases, Gas—gas. Scale bars are shown in each micrograph.

glass films, and glass ingrowths in sulfide grains no larger than a few tenths of a micrometer to a few micrometers. Because of the small sizes of the silicate phases and, hence, the possible interference of the host mineral, we failed to analyze these silicates. However, their analysis in the characteristic radiation of various elements indicates that these phases contain alkalis.

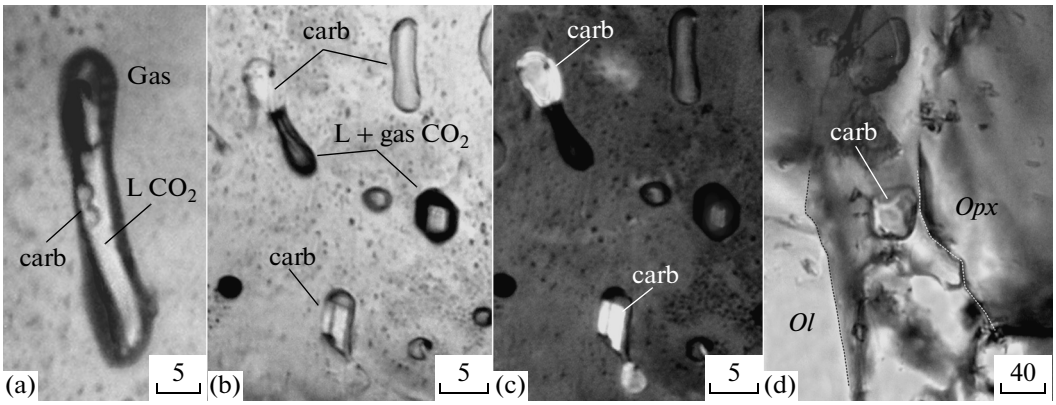

Fig. 3. Micrographs of carbonate-bearing inclusions and interstitial carbonate. (a) Secondary fluid inclusion in orthopyroxene, contains CO_2 (liquid and gas) and two small carbonate crystals on a wall of the vacuole. (b, c) secondary composite inclusions containing carbonate and a fluid phase: (b) parallel polarizers, (c) crossed polarizers. (d) Interstitial material of the xenolith with carbonate crystals. Transmitted light. Scale bars are graduated in micrometers. All symbols as in Fig. 2, carb is carbonate.

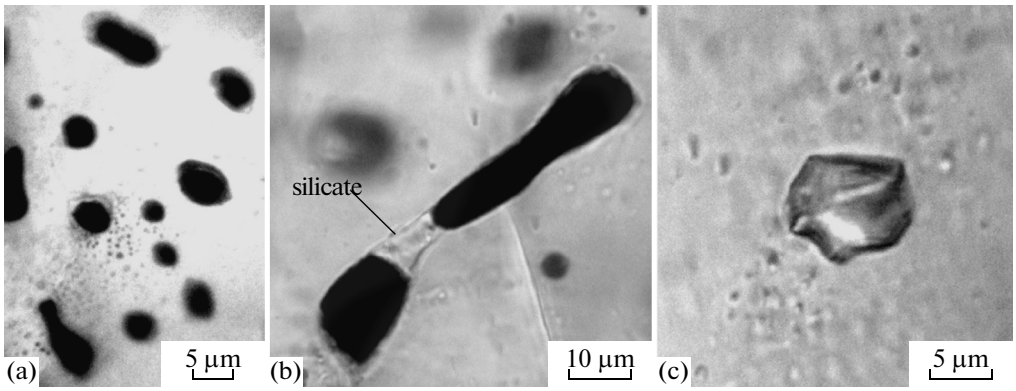

Fig. 4. Micrographs of sulfide–silicate–fluid inclusions in orthopyroxene. (a) Low-magnification micrograph of a group of inclusions. (a) Single inclusion of the group. (c) High-density fluid inclusion ($CO_2 + N_2 + H_2S$) syngenetic with sulfide–silicate inclusions. Transmitted light.

Sulfide phases in mantle xenoliths are described in several papers (for example, in [16, 17]), but fluid-bearing sulfide–silicate (±carbonate) inclusions produced by liquid immiscibility are rare among them [18, 19].

The sulfide–silicate (±carbonate) inclusions coexist with homogeneous (liquid) *fluid inclusions of type V* (Fig. 4c), which have the morphology of negative crystals and are no larger than a few micrometers.

Thermometry of the inclusions. We have examined five melt, 57 fluid, and five composite melt–fluid inclusions in twelve orthopyroxene, olivine, and clinopyroxene phenocrysts. Tables 2 and 3 show the most representative results of cryometric measurements in the inclusions (repeating values were rejected). The measured homogenization temperatures of fluid inclusions in the same series vary because of the partial leaking of the inclusions during decompression and correspond to certain lifting episodes of the xenolith. This means that the measured pressures pertain to the minimum values.

Melt inclusions of type I. Our study of isolated melt inclusions at high temperatures demonstrated that they homogenize at temperatures up to 1000°C, and this value was later used in calculating the pressure under which the fluid inclusion were entrapped.

Inclusions of types II and III (containing much carbon dioxide). When cooled in a microthermometric stage, the material of these inclusions crystallized at temperatures of –96 to –72°C, and the inclusions thereby contained equilibrium CO_2 crystals and gas. The solid phase melted at temperatures of –57.1 to –58.3°C (Table 2), i.e., at temperature below the melting point of pure CO_2 (–56.6°C). This testifies that the inclusions contain subordinate amounts of other volatile components. The homogenization temperature into liquid broadly varies from –44.7 to 29.5°C. The density of fluids in the inclusions studied in orthopyroxene ranges from 0.53 to 1.13 g/cm^3. The fluid pressure calculated for a temperature of 1000°C reaches 11 kbar (Table 2). The fluid of inclusions in olivine and clinopyroxene

Table 2. Representative results of our microthermometric study of fluid inclusions

No.	Mineral	*T*, °C freez.	*T*, °C melt.	*T*, °C hom.	ρ, g/cm^3	*P*, kbar at 1000°C	Note
1	*Opx*	–74.0	–58.1	–44.7	1.13	11.1	Homogeneous (liquid) inclusion
2	*Opx*	–74.0	–58.1	–43.9	1.13	11.0	″
3	*Opx*	–72.0	–57.3	–26.5	1.06	9.0	″
4	*Opx*	–89.0	–57.3	–16.5	1.01	8.0	″
5	*Opx*	–80.1	–58.3	–7.4	0.97	7.0	″
6	*Opx*	–72.0	–58.1	–6.0	0.96	6.9	″
7	*Opx*	–75.3	–58.1	–1.9	0.94	6.5	″
8	*Opx*	–80.1	–58.3	1.3	0.92	6.1	″
9	*Opx*	–94.0	–58.1	22.7	0.74	3.8	″
10	*Opx*	–72.0	–58.1	22.8	0.74	3.8	″
11	*Opx*	–96.0	–58.2	25.7	0.70	3.4	″
12	*Opx*	–82.0	–57.2	28.4	0.65	2.9	″
13	*Opx*	–94.9	–58.2	29.5	0.62	2.7	″
14	*Opx*	–80.1	–57.3	15.6	0.82	4.6	Three-phase inclusion: 2 liquids (CO_2 + H_2O) + gas
15	*Opx*	–74.0	–57.6	–13.6	1.00	7.7	Composite melt–fluid inclusion, two-phase (gas + liquid) fluid
16	*Opx*	–82.8	–57.2	29.1	0.63	2.8	″
17	*Opx*	–82.0	–57.2	30.5	0.57	2.3	″
18	*Cpx*	–82.2	–58.1	7.6	0.88	5.5	Homogeneous (liquid) inclusion, gas hydrate is formed during cooling and melts at 0.7°C
19	*Cpx*	–82.2	–58.1	15.5	0.82	4.6	Homogeneous (liquid) inclusion
20	*Cpx*	–69.2	–57.3	25.9	0.70	3.4	Two-phase (liquid + gas) inclusion
21	*Cpx*	–66.0	–57.3	29.9	0.60	2.6	″
22	*Cpx*	–69.2	–57.3	31.0	0.51	2.0	″
23	*Ol*	–87.0	–57.3	–9.3	0.98	7.2	Homogeneous (liquid) inclusion
24	*Ol*	–88.9	–57.3	–10	0.98	7.3	″
25	*Ol*	–88.0	–57.3	–9.5	0.98	7.2	″
26	*Ol*	–87.3	–57.1	20.3	0.77	4.1	Three-phase (liquid + gas + carbonate crystals) inclusion T, °$C_{freez.}$ is the freezing temperature of inclusions

T, °C, melt. is the melting temperature of CO_2 crystals; *T*, °C, hom. is the homogenization temperature of CO_2 into liquid. Density and pressure were calculated with the FLINCOR software.

Table 3. Data obtained on CO_2–H_2S–N_2 fluid inclusions syngenetic with sulfide–silicate (± carbonate) globules

T, °C, hom.	*T*, °C, melt. CO_2	*T*, °C, phase transitions	Inclusion density, g/cm^3	*P*, kbar, at 1000°C
(–64.0)–(–64.8)	–73.6	(–157)–(–151)	1.15–1.17	11–13

have a density of 0.98 and 0.88 g/cm^3, which corresponds to pressures of 7.3 and 5.5 kbar. In the course of our cryometric measurements, we observed melting of a newly formed phase at a temperature of 0.7°C in one of the cooled fluid inclusions hosted in clinopyroxene. This temperature suggests that CO_2 gas hydrate was formed at a low temperature, i.e., that the fluid contained H_2O.

In the three-phase partly decrepitated inclusions (liquid CO_2 + liquid H_2O + gas), crystallization (freezing) occurred at –74°C, the CO_2 crystals melted at –57.3°C, and the homogenization temperature into

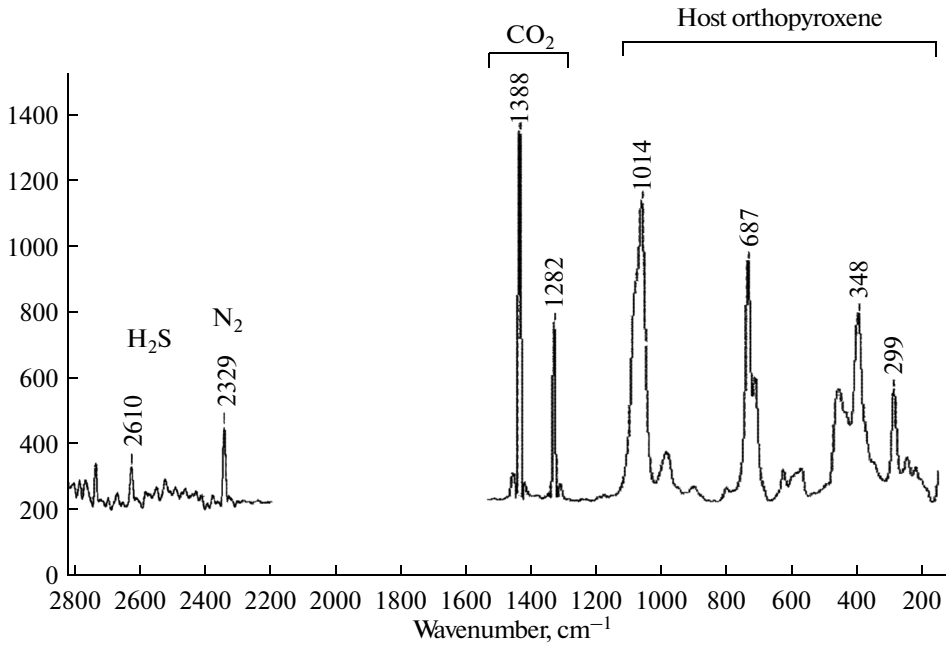

Fig. 5. Raman spectrum of the primary high-density fluid inclusions.

liquid was 15.6°C, which corresponds to a fluid density of 0.83 g/cm^3 and a pressure of 4.6 kbar at 1000°C. Inasmuch as liquid H_2O makes up no more than 0.2 of the vacuole by volume (which is 2–2.5 μm in diameter in its widest section), we failed to measure the freezing temperature of the solution and the melting point of the ice.

In the *composite melt–fluid inclusions (type III)*, the homogenization temperatures of the fluid segregations varied from –13.6 to 30.5°C, the maximum density of the fluid was evaluated at 1.01 g/cm^3 (Table 2), and the pressure was evaluated at 7.7 kbar.

Inclusions of type V. Behavior of the homogeneous (liquid) inclusions coexisting with the sulfide–silicate globules is principally different from those of the inclusions of types II and III (Table 3). The results of our multiple experiments on their cooling and heating can be summarized as follows: (1) When cooled to –56.6°C, the inclusions remained homogeneous (liquid). (2) Gas was detected to appear only when the inclusions were cooled to –77°C. The homogenization temperature into liquid at a cooling rate of 0.5–1°C/min ranged from –64 to –64.8°C, which testifies to a complicated composition of the fluid and its high density. (3) When the inclusions were cooled to temperatures of –80 to –82.2°C, fine-grained aggregates were formed in them, which very rapidly (for less than 1 min) recrystallized into a single crystal. (4) The melting temperature of CO_2 (average of six measurements) was –73.6°C (recall that the melting point of CO_2 at the triple point is –56.6°C). (5) The inclusions were cooled to –180°C. Because of their small sizes and faceted morphology, it was hard to study the inclusions under an optical microscope at still lower temperatures. However, we are confident that certain phase transitions took place in the inclusions at temperatures of –151 to –157°C. Phase transitions in the inclusions at these temperatures (which were close to the critical temperature of N_2: 147.1°C) led us to analyze the composition of the fluid within the framework of the CO_2–N_2 system.

Composition of fluid inclusions. Considering the complicated phase composition of the fluid inclusions, their small sizes, and in certain instances, difficulties in interpretations of the thermodynamic parameters, we have analyzed the inclusions by Raman spectroscopy. The total numbers of the inclusions studied in various minerals were as follows: four in orthopyroxene and two in clinopyroxene, including one three-phase CO_2 inclusion and CO_2-dominated fluid inclusions with and without crystalline phases, one fluid inclusion syngenetic with sulfide–silicate inclusions, and one composite fluid–melt inclusion. We have obtained the following results. The strongest bands in the Raman spectrum of the host orthopyroxene (238, 348, 410, 686, 936, and 1018 cm^{-1}) coincide with those of orthopyroxene in a mantle xenolith from the Bakony–Balaton volcanic field, Hungary [20]. The insignificant deviations from the values reported in this publication seem to be explained by certain differences in the chemistries of the minerals. The spectra of all of the inclusions show pronounced bands typical of CO_2 (1282 and 1385 cm^{-1}) [20–22]. The Raman spectra of the densest fluid inclusions of the earliest episode (Fig. 5) display bands of N_2 (2329–2331 cm^{-1}) and H_2S (2610 cm^{-1}) [21, 23]. The calculated proportions of integral areas of the bands of

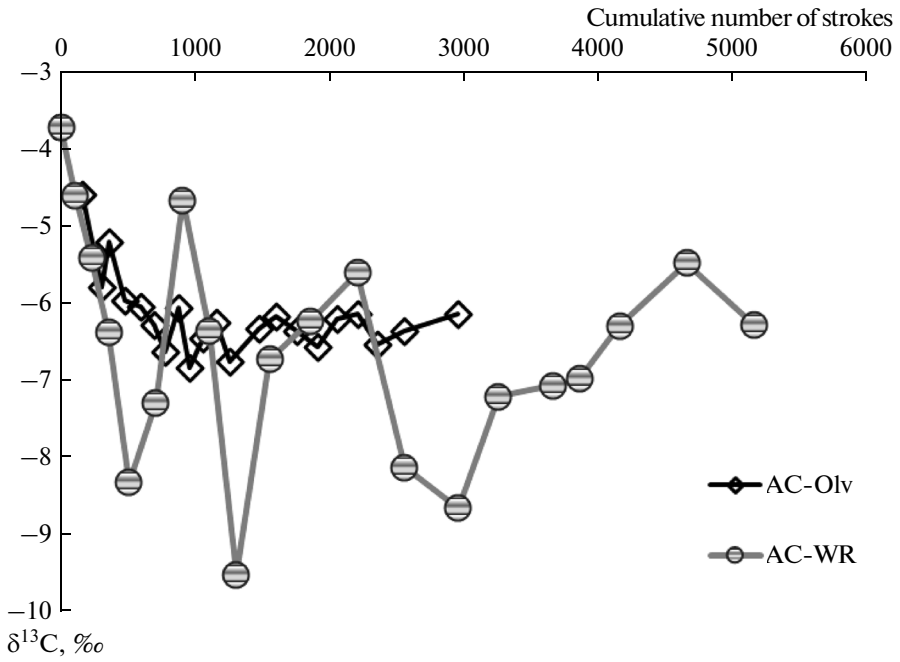

Fig. 6. Variations in the carbon isotopic composition of carbon dioxide depending on the cumulative number of strokes on the whole-rock sample and olivine monomineralic separate.

CO_2 and N_2 in the Raman spectra [24] led us to quantitatively estimate the N_2 mole fraction at 0.1–0.15, is close to the cryometric data.

The Raman spectra of the fluid inclusions of the *younger episode* contain additional bands within the range of 3615–3680 cm^{-1} due to the Raman scattering of O–H in H_2O molecules [25–28]. This is consistent with finds of fluid inclusions with H_2O and CO_2 (analogous to those described above) in which gas hydrate crystallizes. Bands within the range of 3333–33113 cm^{-1} are typical of NH_3 [23, 29, 30]. In a fluid inclusion with small (no larger than 2 μm) crystalline phases, the line at 1097 cm^{-1} corresponds to CO_3^{2-} [20]. The appearance of carbonate in the inclusions can be explained by reaction interaction between CO_2 and the host orthopyroxene composing the walls of the inclusion. We have earlier observed a similar phenomenon when studying CO_2 fluid inclusions in olivine melilitite from Malberg, Germany [31, Fig. 7d]. The possibility of such a reaction in the presence of H_2O has been verified experimentally [32].

Isotopic–Geochemical Study of Inclusions

Our data obtained on the variations in the oxygen and carbon isotopic composition of carbon dioxide extracted from the whole-rock sample and monomineralic olivine separate are summarized in Table 4. Data on the argon and nitrogen isotopic composition and on the helium, argon, carbon, and nitrogen concentrations in the pyroxene separate are presented in Table 5. Note that these data refer to the gases extracted from fluid inclusions by means of stepwise crushing.

CO_2. Upon conducting the isotopic and microthermometric study of the inclusions, we have realized that the xenolith has a uniquely high CO_2 content (>2.7 cm^3/g), which is several times higher than in chilled MORB glasses and in carbonatites [10, 33–35] and more than one order of magnitude higher than the CO_2 contents in mantle xenoliths found elsewhere (see,

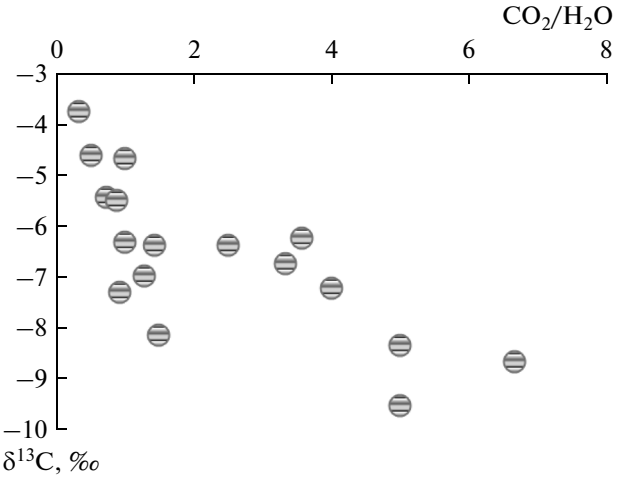

Fig. 7. Correlation between the carbon isotopic composition and the CO_2/H_2O ratio in various stepwise crushing extractions of the whole-rock sample.

Table 4. Carbon and oxygen isotopic composition of carbon dioxide extracted from olivine monomineralic separate and a whole-rock garnet lherzolite sample by stepwise crushing

Cumulative number of strokes	$\delta^{13}C$, ‰ PDB	$\delta^{18}O$, ‰ SMOW	Cumulative number of strokes	$\delta^{13}C$, ‰ PDB	$\delta^{18}O$, ‰ SMOW
Sample/amount of material					
AC-WR/2.0220 g			AC-Olv/0.7747 g		
#50	–3.7	26.7	#200	–4.6	23.5
#150	–4.6	26.3	#350	–5.8	18.6
#275	–5.4	29.1	#400	–5.2	21.4
#400	–6.4	23.1	#520	–6.0	17.0
#550	–8.3	32.1	#640	–6.0	16.1
#750	–7.3	30.9	#740	–6.3	15.5
#950	–4.7	24.1	#820	–6.6	14.2
#1150	–6.4	19.8	#920	–6.1	15.4
#1350	–9.5	16.0	#1000	–6.8	14.0
#1600	–6.7	15.8	#1100	–6.5	15.6
#1900	–6.2	14.8	#1200	–6.3	15.5
#2250	–5.6	14.8	#1300	–6.8	13.7
#2600	–8.1	22.4	#1520	–6.3	14.5
#3000	–8.7	20.8	#1650	–6.2	15.0
#3300	–7.2	10.9	#1800	–6.4	14.2
#3700	–7.1	12.7	#1950	–6.6	13.4
#3900	–7.0	13.5	#2100	–6.2	14.3
#4200	–6.3	24.0	#2250	–6.1	14.4
#4700	–5.5	21.7	#2400	–6.5	12.9
#5200	–6.3	16.0	#2600	–6.4	13.3
			#3000	–6.1	13.0
Average	–6.8	20.8	Average	–6.2	15.5

for example, [36, 37]). The hypothesis that such high CO_2 concentration can occur at deep levels in the Earth finds support in a discovery of an clinopyroxene aggregate of free crystals in mantle rocks and megacrysts with numerous large pores and fluid inclusions with CO_2 of high density in rocks from Shavaryn-Tsayram volcano, Mongolia [18, 38]. The major minerals of the peridotites were found out to contain the liquation type micro- and macro- inclusions presented by fluidized silicate–sulfide melts whose CO_2 concentrations broadly varied from 5.5 to 46 wt %.

The whole-rock sample contains fairly much water (approximately 0.3 wt %) and methane hydrocarbons. The presence of hydrocarbons was confirmed by an CO_2 yield spectrum obtained by passing the gas mixture through a chromatographic column. We have not determined the concentrations of the hydrocarbons quantitatively. The data on the concentrations of the hydrocarbons and their carbon isotopic composition will be obtained in further investigations.

The carbon isotopic composition of carbon dioxide in olivine varies from –4.7 to –6.8‰, and that in the whole-rock sample is from –3.7 to –9.5‰ (Table 4). The spectrum of the variations in the carbon isotopic composition in the whole-rock sample depending on the cumulative number of strokes (Fig. 6) has a complicated sawtooth-shaped form. This may likely be explained by the different susceptibility of the rock-forming minerals of the xenolith (olivine, pyroxenes, and garnet) and the interstitial space to the effect of ball-crushing. As a result of this, larger inclusions in pyroxene shall be opened earlier than those in olivine and garnet. On the other hand, the largest inclusions in various minerals with a high gas pressure to be opened

first. Of course, some part of smaller and lower density inclusions should also be simultaneously opened. In view of this, each crushing step (fraction obtained at this step) corresponds to a mixture of gases from various inclusions, and the gas extraction curve thus reflects mixing of gases extracted from various inclusions and minerals of the xenolith. Note that stepwise crushing does not produce isotopic fractionation, because gas in completely released from the opened inclusions.

The variations in the carbon isotopic composition can be controlled by a number of factors: mixing of material extracted from inclusions of various populations and having different carbon isotopic composition and mixing with other gases (simultaneous opening of variable proportions of primary and secondary inclusions), different susceptibility of minerals to mechanical crushing, variations in the size and density of the fluid inclusions, and fluid content in the interstitial space of the rock. The spectrum of the variations in the carbon isotopic composition in olivine has a simpler shape: the $\delta^{13}C$ variations are not as significant (Fig. 6) and likely suggest that the gas was released from larger and denser primary inclusions during earliest crushing steps and from smaller inclusions (of other genetic nature) during later crushing steps.

Figure 7 shows variations in $\delta^{13}C$ with the CO_2/H_2O ratio for the whole-rock sample. It is worth emphasizing the following tendency: as the CO_2/H_2O ratio increases, the $\delta^{13}C$ decrease from typical mantle values (from −3 to −4‰) to −8...−9‰.

A more clearly pronounced (negative) correlation occurs between the $\delta^{13}C$ values and CO_2 contents (except for three fraction enriched in CO_2): an increase in the CO_2 content is coupled with a decrease in $\delta^{13}C$ (Fig. 8). An analogous tendency was detected for chilled basaltic glasses [34] in which isotopically light ($\delta^{13}C$ less than −7.5‰) carbon of the inclusions can be explained by an admixture of organic carbon from seawater or the material of sediments in subduction zones. The latter mechanism can be considered to be applicable in our case.

The data obtained for the monomineralic olivine separates plot in the top part of the field for the whole-rock sample (Fig. 8). Note that isotopically heavy carbon was obtained in the first crushing steps of both the whole-rock sample and the olivine separate. Carbon of such isotopic composition is typical for CO_2 in bubbles from MORB chilled glasses ($\delta^{13}C$ close to −4‰, according to [34, 39–41]) and fluid inclusions in mantle xenoliths [36]. Later crushing steps for both samples yielded CO_2 with isotopically lighter carbon. The weighted mean $\delta^{13}C$ values of the whole-rock sample and monomineralic separate are somewhat different ($\delta^{13}C_{WR} = -6.8$‰ and $\delta^{13}C_{Px} = -6.2$‰) but generally fall within the ranges typical for mantle rocks.

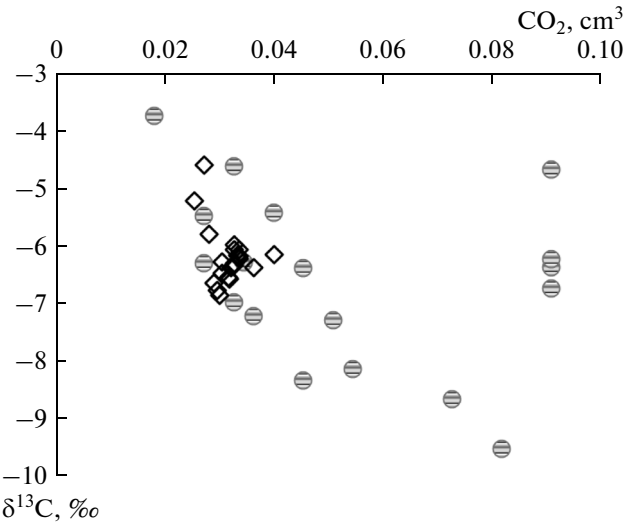

Fig. 8. Correlation between the carbon isotopic composition and the carbon dioxide content in various stepwise crushing fractions in the whole-rock sample (⛀ AC-WR) and olivine monomineralic separate (◇ AC-Olv).

He, Ar, N_2, and C. We have obtained data on the isotopic composition of Ar and N_2, and concentrations of He and C only for the pyroxene, because (as was mentioned above) the data on the whole-rock sample can be compromised by simultaneous gas extraction from different minerals and from interstitial space. The sample demonstrates very high contents of carbon in the form of carbon dioxide (see above) and argon and relatively low concentrations of nitrogen and helium (Table 5).

Figure 9 shows the release curves of specific (normalized to the cumulative number of strokes at each step) He, Ar, N_2 and CO_2 (C) yield obtained during stepwise crushing. Noble gases and nitrogen exhibit a similar systematic decrease in their normalised concentrations from the fractions of the first crushing steps to the last ones. The specific C amount in the form of CO_2 increases in the first four stepwise crushing fractions and then starts gradually decreasing. This behavior of the gases is explained by their genetic features and the *PVT* parameters of fluids in the inclusions. As we determined the first fluid portions that had entered the mantle source rocks had been entrapped as high-pressure inclusions. At crushing-extractions temperatures of 120–140°C, the pressure in the vacuoles was very high and could reach 4 kbar. These gases should have been released during the very first strokes. Because all of the inclusions contain large amounts of CO_2, the increase in the concentrations affected only C (CO_2). During the later crushing steps, the number of smaller inclusions of lower density that were thereby opened increased. These inclusions are typical for the fluids of the late generations, and Raman spectroscopic data indicate that CO_2 in these inclusions are strongly dominates over

Table 5. Concentrations, isotopic composition, and elemental ratios of helium, carbon, nitrogen, and argon in stepwise crushing extractions from a monomineralic pyroxene separate from the garnet lherzolite

Cumulative number of strokes	^4He, 10^{-8} cm^3/g	C, ng	N, ng	^{40}Ar, 10^{-8} cm^3/g	$\delta^{15}N$, ‰ atm	(±)	$^{40}Ar/^{36}Ar$	(±)	$^4He/^{40}Ar^*$	N_2/Ar
Xenolith AC Px (0.526 g)										
#300	7.4	14815	108	197	2.05	0.28	533	10	0.1	31
#450	2	11958	18	30	–2.57	0.28	497	9	0.2	34
#700	1.8	30069	20	33	0.74	2.33	510	10	0.1	33
#1000	1.5	65371	14	24	0.89	0.26	498	9	0.2	34
#1500	1.6	88732	13	20	1.24	0.27	513	9	0.2	38
#2300	1.9	147209	16	19	–0.38	0.04	482	12	0.3	47
#3300	1.9	162409	15	13	–0.72	0.15	461	11	0.4	65
#4800	2.1	149602	21	13	–1.54	0.46	437	8	0.5	86
#7000	2.1	76362	23	15	–2.28	0.26	370	7	0.7	86
Total/Average	**22.3**	**746527**	**248**	**364**	**0.47**	**0.48**	**509**	**9**	**0.1**	**38**

all other gases, N_2 inclusive. This fact is fully corroborated by isotopic–geochemical data: the C/Ar and C/N_2 ratios systematically increase from earlier to later crushing steps of pyroxene monomineralic separate, up to #3300 strokes (Fig. 10). A similar situation was observed in the late stage carbonatites at the Guli Massif. These rocks were significantly metasomatized, and one of the agents of this metasomatism is thought to have been meteoric waters [33]. During the latest crushing steps, the C/Ar and C/N_2 ratios decreased (#4800 and #7000 strokes, Fig. 10), likely because of a decrease in the amount of CO_2 and underestimated blanks for Ar and N_2. Note that the release of CO_2 from inclusions in the pyroxene was not complete even after 7000 strokes, judging from the fact that much of this gas was still released during the latest strokes. A portion of the crushing material remaining after step-crushing was later studied by means of compete melting, which has shown that the material contained as much as 0.6 wt % of carbon (at 0.14% extracted by stepwise crushing). This

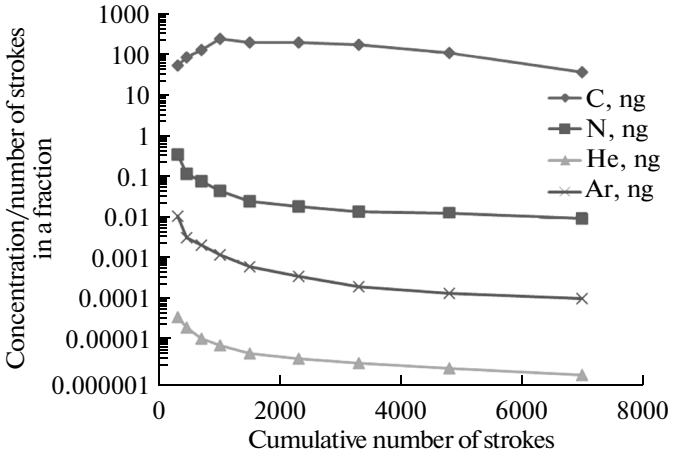

Fig. 9. Specific yields of the gases in stepwise crushing fractions of the pyroxene monomineralic separate.

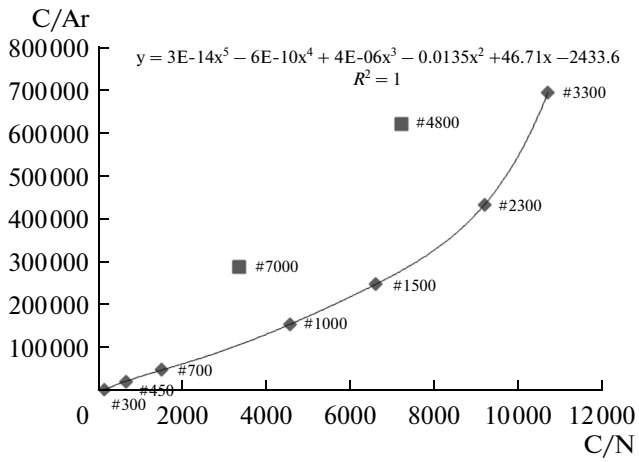

Fig. 10. Correlation between the C/N and C/Ar ratios in stepwise crushing fractions of the monomineralic pyroxene separate. The sign # denotes the cumulative number of strokes on the sample.

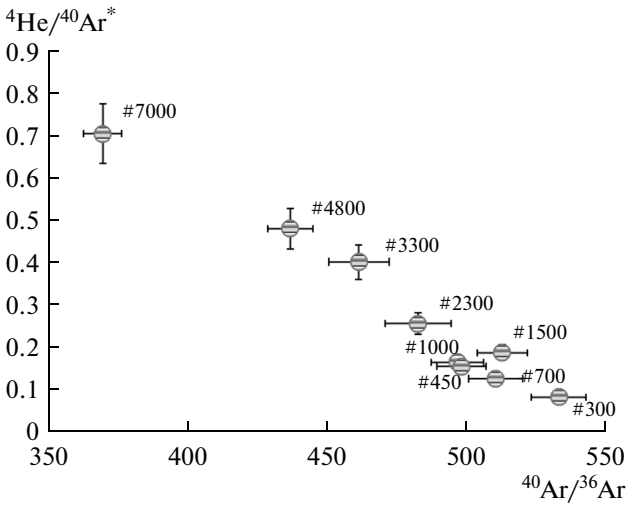

Fig. 11. Correlation between the $^4He/^{40}Ar^*$ and $^{40}Ar/^{36}Ar$ ratios in stepwise crushing fractions of the monomineralic pyroxene separate. The sign # denotes the cumulative number of strokes on the sample.

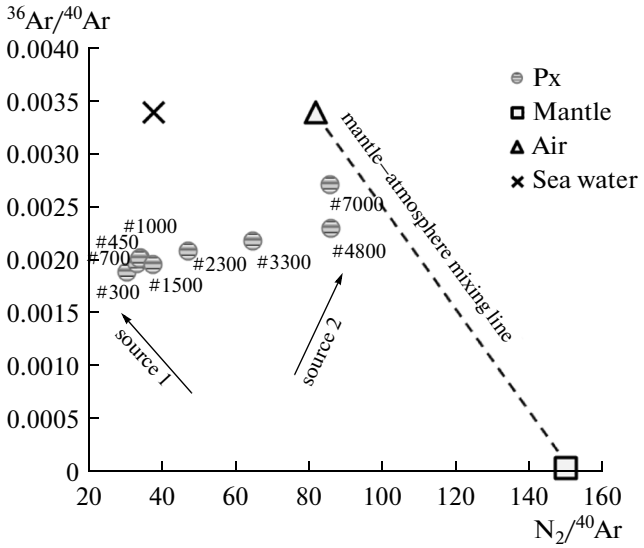

Fig. 12. $^{36}Ar/^{40}Ar$–$N_2/^{40}Ar$ diagram for stepwise crushing fractions of the monomineralic pyroxene separate. Data suggest mixing of two sources, one of which (source 2) resulted from simple two-component mantle–atmosphere mixing; its composition is characterized by the gases released during the latest crushing steps from the less dense and smallest inclusions. The composition of source 1 cannot be explained by simple mixing of any known reservoirs and is characterized by gases released during the earliest crushing steps from the largest and highest pressure inclusions.

extremely high CO_2 content in the crushed pyroxene may likely be explained by the occurrence of carbonates in the secondary inclusions (Figs. 3a, 3b, 3c) and interstitial space of the peridotite (Fig. 3e).

The $^4He/^{40}Ar^*$ ratio (where $^{40}Ar^* = {}^{40}Ar_{measured} - {}^{36}Ar_{measured} \times 295.5$) increases from 0.1 to 0.7 from the earliest to latest crushing steps (Fig. 11, Table 5). These values are several times different from the calculated mantle values (1.6–4), which suggests that an element fractionation took place during the metasomatic alteration of the mantle source material. It is known that such alteration is typical for mantle xenoliths representing the material of the subcontinental lithospheric mantle [9, 42]. The fractionation of elements could occur during the reaction melting of the mantle source material with the derivation of melt portions in equilibrium with fluid, that is supported by findings of syngenetic melt and fluid inclusions. He, whose solubility in melt is ten times higher than that of Ar [43], thereby enriched the melt, whereas Ar was preferably lost to the gas phase. As a result, inclusions in the pyroxene were enriched in Ar with respect to He.

In contrast to He, N_2 and Ar have roughly equal solubilities in basaltic melt [44], and the N_2/Ar ratios should have not very significantly in the course of melt degassing. However, from earlier to later crushing steps, this ratio increases by a factor as high as almost three (Table 5). Moreover, the N_2/Ar ratio is correlated with the $^{36}Ar/^{40}Ar$ ratio (and hence, is negatively correlated with the $^{40}Ar/^{36}Ar$ ratio, which is a criterion of the mantle provenance and the degree of contamination with atmospheric gases) in fractions from different crushing steps (Fig. 12). Such significant variations in the Ar isotopic composition cannot be explained by isotopic fractionation during melt degassing. In our situation, this testifies that the xenolith was affected by genetically distinct fluids in the course of its metasomatic transformations and, consequently, entrapped genetically distinct inclusions with different element and isotopic ratios. As is shown in Fig. 12, it is logical to suggest at least two distinct fluid sources. One of them had low $^{40}Ar/^{36}Ar$ and N_2/Ar ratios, which were close to those in seawater (–38). Furthermore, fluids from this source have low $^4He/^{40}Ar^*$ (Fig. 11), C/N, and C/Ar (Fig. 10) ratios typical for mantle xenoliths and isotopically heavy nitrogen (Figs. 13, 14). A similar nitrogen isotopic composition was found in fluid inclusions in carbonatites from the Guli Massif [33, 35] and xenoliths from Dreiser Weiher volcano, Germany [37]. This source is represented by the largest high-pressure inclusions [45], which are opened during early crushing steps. The second episode of fluid processing of the mantle peridotite was responsible for inclusions with the highest CO_2 contents and close to the atmospheric $^{40}Ar/^{36}Ar$ (295.5) and N_2/Ar (83) ratios. As can be seen in the Ar and N_2 isotope diagrams (Figs. 12–14), these fluids are mixtures of the mantle MORB source and atmospheric gases, with the predominant contribution of the atmospheric Ar and N_2 components.

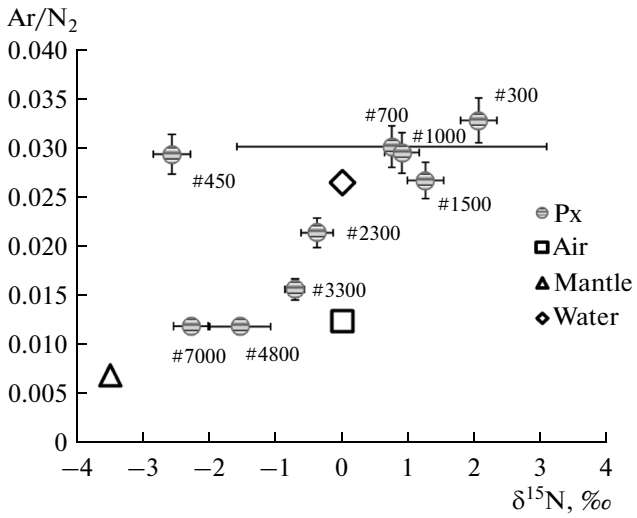

Fig. 13. Variations in the nitrogen isotopic composition and the Ar/N_2 ratio of the stepwise crushing fractions of the monomineralic pyroxene separate. Except a single data point, all data show systematic variations from earliest to latest crushing steps, suggesting mixing of two sources, one of which resulted from simple two-component mixing of the mantle and atmosphere (see above).

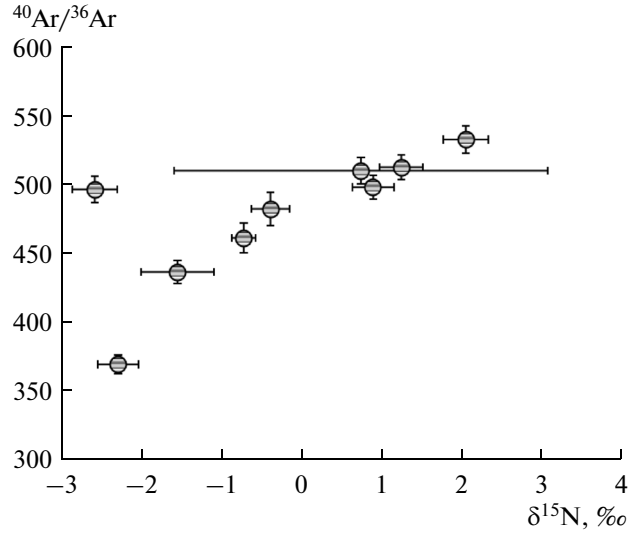

Fig. 14. Correlation between the argon and nitrogen isotopic compositions in stepwise crushing fractions of the monomineralic pyroxene separate.

CONCLUSIONS

Our data obtained on the garnet lherzolite show that the rock is rich in fluids. The effect of heat–fluid fluxes on the mantle source material resulted in its profound metasomatic recycling. In the course of this process, minerals of the peridotite entrapped primary and secondary fluid inclusions of various populations. Our data reveal at least two episodes of fluid recycling. The fluids of the earlier episode had the most complicated composition and were entrapped under a high pressure (>13 kbar). They can be provisionally classified into two subgroups. One of them comprises CO_2-dominated fluid with relatively high concentrations of other volatile components: 0.1–0.2 mole fractions of N_2 and, perhaps, also H_2S and H_2O. These fluids are components of unique carbonate–sulfide inclusions produced by liquid immiscibility. The possibility that such inclusions can occur in the upper mantle was demonstrated in [19, 38, 39, 46, 47]. The fluids of the other subgroup of the earlier episode contain admixtures of analogous volatile compounds, their CO_2 concentrations are much higher than in the other subgroup, and the H_2S and N_2 concentrations are much lower. Their Raman spectra contain N–H bands (NH_3 at 3313 cm^{-1}). The fluids of the younger second episode (entrapped under pressures ≤7 kbar) contain much higher concentrations not only of CO_2 but also of H_2O (up to pure H_2O inclusions and the formation of CO_2 gas hydrate in the inclusions cooled by liquid N_2).

Even a brief review of literature data on the composition of fluids in the Earth's mantle confirms that these fluids are dominated by CO_2 (see, for example, [18, 45, 46, 48, 49]). Much more rarely these fluids contain admixtures of volatile components of the more complicated COHNS system, such as H_2S [50–52], SO_2 [53], CO [21], and N_2 [54–56]. It is also known that N_2 is a typical admixture in diamonds. It has been experimentally demonstrated in [56] that nitrogen can occur in the mantle as either NH_3 or N_2 in mixture with H_2 depending on temperature and pressure. The ability of nitrogen to form various species is of particular interest in view of the fact that NH_4^+ can play a role of an equivalent of K^+. For instance, we have found nitrogen in melt and in fluid inclusions in minerals from a K-enriched rock: lamproite from Australia [57]. Finds of H_2O-bearing mantle fluids are still scarce rare? [52, 58].

Although the contribution of such volatile components as N_2, NH_3, H_2S, and H_2O to the overall budget of deep fluids is relatively low, these components play an important part in the processes of mantle metasomatism, and this is reflected in the geochemistry of the derived magmas. It has been demonstrated that not only H_2O but also other volatile components are able to transport perceptible amounts of ore-forming metals and REE [26, 48, 51, 59], and this is corroborated by data on the mineralogy of the xenolith [4].

The influx of hot deep fluids was responsible not only for metasomatic processes but also for reaction-driven melting and recrystallization of the mantle material. This follows from the occurrence of crystalline and melt inclusions in the major rock-forming minerals of the lherzolite and from traces of resorption of clinopyroxene crystals and incipient melt generation. When cooled, this melt gave rise to newly formed phases in the interstitial space [4].

Two episodes of fluid-mediated reworking of the mantle material are also confirmed by isotope-geochemical data. The high-pressure fluid inclusions of the first episode have low C/N_2, C/Ar, and N_2/Ar ratios, $\delta^{13}C$ of CO_2 similar to those typical of MORB chilled glasses, isotopically heavy N_2, and somewhat elevated (to 530) $^{40}Ar/^{36}Ar$ ratios.

The late-stage fluids are present in the secondary inclusions, which occur as composite varieties with carbonate. They typically have higher (by two to three orders of magnitude) C/N_2 and C/Ar ratios, lower $\delta^{13}C$ in CO_2, and N_2/Ar and $^{40}Ar/^{36}Ar$ ratios close to the atmospheric values. The isotopic composition and elemental ratios of Ar and N_2 led us to suggest that the late-stage fluids could have been produced by two-component mixing, with more than 95% of the atmospheric component. Regarding the low (compared to the mantle values) $^{40}Ar/^{36}Ar$ ratios in the early-stage fluids, the percentage of atmospheric Ar could have been also fairly high. However, the N_2/Ar ratio (31) is almost three times lower than the atmospheric one (the estimated value of the mantle is 150 [60]). Among known global reservoirs, it is the closest to the value of seawater (38, according to [60]). The late-stage fluids contain isotopically heavy nitrogen, whose $\delta^{15}N$ falls into the field of values typical for mantle xenoliths of Dreiser Weiher volcano, Pannonian Basin [37], and carbonatites of the Guli Massif [33, 35] and the Kola Peninsula [61]. Some researchers [60, 61] believe that positive $\delta^{15}N = 2–3$ are typical of mantle plumes OIB sources. However, our data indicate that this nitrogen isotopic composition can correspond to carbonatites and mantle xenoliths from continental rifting zones. In our opinion, the low $^{40}Ar/^{36}Ar$ ratios, which are typical for the mantle, can be explained by a subductional nature of the fluids.

ACKNOWLEDGMENTS

The authors thank the O.V. Kuznetsova and V.S. Sevast'yanov of the laboratory of Carbon Geochemistry at the Vernadsky Institute of Geochemistry and Analytical Chemistry, Russian Academy of Sciences, for assistance in conducting isotopic analysis of carbon and oxygen in carbon dioxide. This study was financially supported by the Russian Foundation for Basic Research (project nos. 09-05-00678a, 13-05-01009a, and 13-05-00499a) and Program 4 ONZ RAS.

REFERENCES

1. I. H. Campbell and R. W. Griffiths, "Implications of mantle plume structure for the evolution of flood basalts," Earth Planet. Sci. Lett. **99**, 79–93 (1990).
2. L. N. Kogarko, "Alkaline magmatism and enriched mantle reservoirs: mechanisms, time, and depth of formation," Geochem. Int., **44** (1), 3–10 (2006).
3. A. W. Hofmann, "Mantle geochemistry: The message from oceanic volcanism," Nature **385**, 219–229 (1997).
4. L. N. Kogarko, G. Kurat, and T. Ntaflos, "Henrymeyerite in the metasomatized upper mantle of eastern Antarctica," Can. Mineral. **45**, 497–501 (2007).
5. P. Sarda, Th. Staudacher, and C. J. Allegre, "$^{40}Ar/^{36}Ar$ in MORB glasses: constraints on atmosphere and mantle evolution," Earth Planet. Sci. Lett. **72**, 357–375 (1985).
6. T. Staudacher, P. Sarda, S. H. Richardson, C. J. Allegre, I. Sagna, and L. V. Dmitriev, "Noble gases in basalt glasses from a Mid-Atlantic Ridge topographic high at ^{14}N: Geodynamic consequences," Earth Planet. Sci. Lett. **96**, 119–133 (1989).
7. M. Trieloff, J. Kunz, D. A. Clague, D. Harrison, and C. J. Allegre, "The nature of pristine noble gases in mantle plumes," Science **288**, 1036–1038 (2000).
8. J. Hopp, M. Trieloff, and R. Altherr, "Neon isotopes in mantle rocks from the Red Sea region reveal large-scale plume–lithosphere interaction," Earth Planet. Sci. Lett. **219**, 61–76 (2004).
9. A. I. Buikin, M. Trieloff, J. Hopp, T. Althaus, E. V. Korochantseva, W. H. Schwarz, and R. Altherr, "Noble gas isotopes suggest deep mantle plume source of Late Cenozoic mafic alkaline volcanism in Europe," Earth Planet. Sci. Lett. **230**, 143–162 (2005).
10. A. I. Buikin, Yu. A. Nevinny, V. I. Ustinov, V. A. Grinenko, E. P. Smirnova, V. S. Sevast'yanov, E. V. Korochantseva, and S. A. Silantyev, "High-vacuum device for study of isotope composition of light elements from fluid inclusions in mantle rocks by step crushing," Elektron. Nauchn. Inform. Zh. Vestn. Otd. Nauk Zemle RAN, No. 2 (2010).
11. A. B. Verchovsky, M. A. Sephton, I. P. Wright, and C. T. Pillinger, "Separation of planetary noble gas carrier from bulk carbon in enstatite chondrites during stepped combustion," Earth Planet. Sci. Lett. **199**, 243–255 (2002).
12. T. Morishita, S. Arai, and F. Gervilla, "High-pressure aluminous mafic rocks from the Ronda peridotite massif, southern Spain: significance of sapphirine- and corundum-bearing mineral assemblages," Lithos **57**, 143–161 (2001).
13. C. Ballhaus, M. Tredoux, and A. Spath, "Phase relations in the Fe–Ni–Cu–PGE–S system at magmatic temperature and application to massive sulphide ores of the Sudbury Igneous Complex," J. Petrol. **42** (10), 1911–1926 (2001).
14. G. Kullerud, R. A. Yund, and G. H. Moh, "Phase relations in the Cu–Fe–S, Cu–Ni–S, and Fe–Ni–S systems," Econ. Geol. **4**, 323–343 (1969).
15. J. Guo, W. Griffin, and S. O'Reilly, "Geochemistry and origin of sulphide minerals in mantle xenoliths: Qilin, southeastern China," J. Petrol. **40** (7), 1125–1149 (1999).
16. J. P. Lorand, "Abundance and distribution of Cu–Fe–Ni sulfides, sulfur, copper and platinum-group elements in orogenic-type spinel lherzolite massifs of Arirge (northeastern Pyrenees, France)," Earth Planet. Sci. Lett. **93**, 50–64 (1989).
17. Z. Zajacz and C. Szabo, "Origin of sulfide inclusions in cumulate xenoliths from Nograd-Gomor volcanic

field, Pannonian Basin (north Hungary/south Slovakia)," Chem. Geol. **194**, 105–117 (2003).

18. V. I. Kovalenko, I. P. Solovova, V. B. Naumov, D. A. Ionov, and A. I. Tsepin, "Mantle mineral formation with participation of CO_2–sulfide–silicate fluid," Geokhimiya, No. 3, 289–303 (1986).
19. T. Andersen, W. Griffin, and S. Y. O'Reilly, "Primary sulphide melt inclusions in mantle-derived megacrysts and pyroxenites," Lithos **20**, 279–294 (1987).
20. M. Berkesi, T. Guzmics, C. Szabo, J. Dubessy, R. Bodnar, K. Hidas, and K. Ratter, "The role of CO_2-rich fluids in trace element transport and metasomatism in the lithospheric mantle beneath the central Pannonian Basin, Hungary, based on fluid inclusions in mantle xenoliths," Earth Planet. Sci. Lett. **331–332**, 8–20 (2012).
21. S. C. Bergman and J. Dubessy, "CO_2–CO fluid inclusions in a composite peridotite xenolith: Implications for upper mantle oxygen fugacity," Contrib. Mineral. Petrol. **85**, 1–13 (1984).
22. R. Bonelli and M. L. Frezzotti, *Raman Spectra Database*, (2003). http://www.dst.unisi.it/geofluids-lab/Raman%20intro.htm.
23. M. L. Frezzotti, F. Tecce, and A. Casagli, "Raman spectroscopy for fluid inclusion analysis," J. Geochem. Explor. **112**, 1–20 (2012).
24. J. Dubessy, B. Poty, and C. Ramboz, "Advances in C–O–H–N–S fluid geochemistry based on micro-Raman spectrometric analysis of fluid inclusions," Eur. J. Mineral. **1**, 517–534 (1989).
25. K. M. Rosso and R. J. Bodnar, "Microthermometric and Raman spectroscopic detection of CO_2 in fluid inclusions and Raman spectroscopic characterization of CO_2," Geochim. Cosmochim. Acta **59**, 3961–3975 (1995).
26. M. L. Frezzotti and A. Peccerillo, "High flux of (diamond CO_2–H_2O–H_2S) fluids in the mantle beneath Hawaii: evidence from fluid inclusions in garnet pyroxenites from Salt Lake Crater (Oahu, Hawaii)," AGU-Meeting Abstract, #V33D-08, (2005).
27. Q. Sun, "The Raman OH stretching bands of liquid water," Vib. Spectrosc. **51**, 213–217 (2009).
28. A. G. Simakin, "The role of intercameral degassing of andesite magma of the Shiveluch Volcano (Kamchatka)," Dokl. Earth Sci. **431** (2), 458–461 (2010).
29. R. G. Dickinson, R. T. Dillon, and F. Rasetti, "Raman spectra of polyatomic gases," Phys. Rev. **34**, 582–590 (1929).
30. F. Rossetti, F. Tecce, L. Aldega, M. Brilli, and C. Faccenna, "Deformation and fluid flow during orogeny at the palaeo-Pacific active margin of Gondwana: the Early Palaeozoic Robertson Bay accretionary complex (North Victoria Land, Antarctica)," J. Metamorph. Geol. **24**, 33–53 (2006).
31. I. P. Solovova, A. V. Girnis, I. T. Rass, N. N. Kononkova, and I. Keller, "Composition and evolution of fluid-saturated calcium-rich melts: Inclusions in the minerals of olivine melilitite from Mahlberg, Rhine Graben," Geochem. Int. **43** (9), 843–861 (2005).
32. B. Yu. Sushentsova, S. N. Shilobreeva, and D. V. Grichuk, "Experimental and thermodynamic modeling of CO_2 interaction with olivine at temperature 250°C and pressures up to 30 atmospheres," in *Proceedings of Conference on "Physicochemical and Petrophysical Studies in Earth's Science," Moscow, Russia, 2007* (Moscow, 2007), pp. 126–130 [in Russian].
33. A. I. Buikin, A. B. Verchovsky, and L. N. Kogarko, "New data on element and isotope composition of fluid inclusions in carbonatites and ultrabasic rocks of the Guli Massif," in *Proceedings of Conference on "Ore Potential of Alkaline, Kimberlite, and Carbonatite Magmatism, Moscow, Russia, 2012"* (Moscow, 2012), pp. 22–24 (2012).
34. A. I. Buikin, A. B. Verchovsky, V. A. Grinenko, S. A. Silant'ev, V. S. Sevast'yanov, Yu. A. Nevinnyi, and E. P. Smirnova, "C, N, He, and Ar isotope and element ratios in fluid inclusions from MORB chilled glasses: stepwise crushing data," Geochem. Int. **51**, No. 4, 338–344 (2013).
35. A. I. Buikin, A. B. Verchovsky, V. A. Grinenko, and L. N. Kogarko, "The first stepwise crushing data on C, N and Ar isotopic and elemental ratios in Guli carbonatites," in *Abstracts of 21st Goldschmidt Conference, Prague, 2011* (Prague, 2011), # A596.
36. T. Trull, S. Nadeau, F. Pineau, M. Polve, M. Javoy, "C–He systematic in hotspot xenoliths: Implications for mantle carbon contents and carbon recycling," Earth Planet. Sci. Lett. **118**, 43–64 (1993).
37. A. I. Buikin and A. B. Verchovsky, "C, N_2, He, Ar in fluid inclusions from mantle xenoliths of the Dreiser Weiher (Germany) and Szentbekkalla (Hungary) volcanoes," in *Proc. ESEMPG*, 21 (2013).
38. V. I. Kovalenko, A. I. Tsepin, D. A. Ionov, and I. D. Ryabchikov, "Garnet–pyroxene druse—an example of fluid crystallization in mantle," Dokl. Akad. Nauk SSSR **280**, (2), 449–453 (1985).
39. F. Pineau, S. Shilobreeva, R. Hekinian, D. Bideau, and M. Javoy, "Deep-sea explosive activity on the Mid-Atlantic Ridge near 34°50′ N: A stable isotope (C, H, O) study," Chem. Geol. **211**, 159–175 (2004).
40. T. P. Fischer, P. Burnard, B. Marty, J. M. de Moo, D. R. Hilton, A. M. Shaw, P. H. Barry, C. Ramirez, and F. Mangasin, "Oldoinyo Lengai gas chemistry from 2005 to 2009: Insights to carbonatite–nephelinite volcanism," in *AGU Fall Meeting, San Francisco, 2009* (San Francisco, 2009), # 1: 06.
41. M. Javoy and F. Pineau, "The volatiles record of a 'popping' rock from the Mid-Atlantic Ridge at 14° N: Chemical and isotopic composition of gas trapped in the vesicles," Earth Planet. Sci. Lett. **107**, 598–611 (1991).
42. T. Dunai and H. Baur, "Helium, neon, and argon systematics of the European subcontinental mantle: implications for its geochemical evolution," Geochim. Cosmochim. Acta **59**, 2767–2783 (1995).
43. M. R. Carroll and D. S. Draper, "Noble gases as trace elements in magmatic processes," Chem. Geol. **117**, 37–56 (1994).
44. B. Marty and L. Zimmermann, "Volatiles (H, C, N, Ar) in Mid-Ocean Ridge basalts: assessment of shallow-level fractionation and characterization of source composition," Geochim. Cosmochim. Acta **63**, 3619–3633 (1999).
45. I. P. Solovova, V. B. Naumov, V. I. Kovalenko, A. V. Girnis, and A. V. Guzhova, "History of formation of spinel lherzolite (Dreiser Weiher, Germany) based on micro-

inclusion study," Geokhimiya, No. 10, 1400–1411 (1990).
46. T. Andersen and E.-R. Neumann, "Fluid inclusions in mantle xenoliths," Lithos **55**, 301–320 (2001).
47. H. E. F. Amundsen, "Evidence for liquid immiscibility in the upper mantle," Nature, No. 327, 692–695 (1987).
48. J. M. Rosenbaum, A. Zindler, and J. L. Rubenstone, "Mantle fluids: evidence from fluid inclusions," Geochim. Cosmochim. Acta **60** (17), 3229–3252 (1996).
49. M. L. Frezzotti, J. L. R. Touret, and E.-R. Neumann, "Ephemeral carbonate melts in the upper mantle: carbonate-silicate immiscibility in microveins and inclusions within spinel peridotite xenoliths, La Gomera, Canary Islands," Eur. J. Mineral. **14**, 891–904 (2002).
50. K. Hidas, T. Guzmics, Cs. Szabo, I. Kovacs, R. J. Bodnar, Z. Zajacz, Zs. Nedli, L. Vaccari, and A. Perucchi, "Coexisting silicate melt inclusions and H_2O-bearing, CO_2-rich fluid inclusions in mantle peridotite xenoliths from the Carpathian–Pannonian region (central Hungary)," Chem. Geol. **274**, 1–18 (2010).
51. C. Szabo, M. Berkesi, K. Hidas, T. Guzmics, R. J. Bodnar, and J. Dubessy, "Trace element transport by COHS fluids in the deep lithosphere: A fluid inclusion perspective," Abstr. Goldschmidt Conference, A1016 (2010).
52. Zs. Pinter, I. Kovacs, M. Berkesi, Cs. Szabo, Djoukam J. F. Tene, J.-P. Tchouankoue, and A. Perucchi, "Unique, phlogopite- and amphibole-bearing fluid inclusions in upper mantle xenoliths from Cameroon Volcanic Line," Abstr. ECROFI-XXI, 158–159 (2011).
53. R. Kaldos, M. Berkesi, K. Hidas, K. Yang, and Cs. Szabo, "CO_2–SO_2–H_2O fluid inclusions in peridotite xenoliths from Jeju Island (South Korea)," Abstr. ECROFI-XXI, 112–113 (2011).
54. J. Touret, "An empirical phase diagram for a part of the N_2–CO_2 system at low temperature," Chem. Geol. **37**, 49–58 (1982).
55. T. Andersen, E. A. J. Burke, and E.-R. Neumann, "Nitrogen-rich fluid in the upper mantle: Fluid inclusions in spinel dunite from Lanzarote, Canary Islands," Contrib. Mineral. Petrol. **120**, 20–28 (1995).
56. Y. Li, H. Keppler, and A. Audetat, "Nitrogen speciation in mantle fluids," Mineral. Mag. **75**, 1322 (2011).
57. I. D. Ryabchikov, I. P. Solovova, N. V. Sobolev, et al., "Nitrogen in lamproitic magmas," Dokl. Akad. Nauk SSSR **288** (4), 976–979 (1986).
58. M. Berkesi, K. Hidas, T. Guzmics, J. Dubessy, R. J. Bodnar, C. Szabo, B. Vajnad, T. Tsunogae, "Detection of small amounts of H_2O in CO_2-rich fluid inclusions using Raman spectroscopy," J. Raman Spectrosc. **40**, 1461–1463 (2009).
59. R. Giere, "Transport and deposition of REE in H_2S-rich fluids: Evidence from accessory mineral assemblages," Chem. Geol. **110**, 251–268 (1993).
60. B. Marty and N. Dauphas, "The nitrogen record of crust–mantle interaction and mantle convection from Archean to present," Earth Planet. Sci. Lett. **206**, 397–410 (2003).
61. N. Dauphas and B. Marty, "Heavy nitrogen in carbonatites of the Kola Peninsula: A possible signature of the deep mantle," Science **286**, 2488–2490 (1999).

Translated by E. Kurdyukov